

Fast Geometric Learning of MIMO Signal Detection over Grassmannian Manifolds

Rashed Shelim^{*†}, Walid Saad^{*}, and Naren Ramakrishnan[†]

^{*}Department of Electrical and Computer Engineering, Virginia Tech, USA

[†]Department of Computer Science, Virginia Tech, Arlington, VA 22203

Emails: {rasheds@vt.edu, walids@vt.edu, naren@vt.edu}

Abstract—Domain or statistical distribution shifts are a key staple of the wireless communication channel, because of the dynamics of the environment. Deep learning (DL) models for detecting multiple-input multiple-output (MIMO) signals in dynamic communication require large training samples (in the order of hundreds of thousands to millions) and online retraining to adapt to domain shift. Some dynamic networks, such as vehicular networks, cannot tolerate the waiting time associated with gathering a large number of training samples or online fine-tuning which incurs significant end-to-end delay. In this paper, a novel classification technique based on the concept of geodesic flow kernel (GFK) is proposed for MIMO signal detection. In particular, received MIMO signals are first represented as points on Grassmannian manifolds by formulating basis of subspaces spanned by the rows vectors of the received signal. Then, the domain shift is modeled using a geodesic flow kernel integrating the subspaces that lie on the geodesic to characterize changes in geometric and statistical properties of the received signals. The kernel derives low-dimensional representations of the received signals over the Grassman manifolds that are invariant to domain shift and is used in a geometric support vector machine (G-SVM) algorithm for MIMO signal detection in an unsupervised manner. Simulation results reveal that the proposed method achieves promising performance against the existing baselines like OAMPnet and MMNet with only 1,200 training samples and without online retraining.

Index Terms—Dynamic wireless networks, domain shift, geodesic flow kernel, Grassmannian manifolds, MIMO signal detection.

I. INTRODUCTION

Signal detection under rapid domain shift (e.g., distribution shift) is one of the fundamental problems in dynamic wireless networks, such as vehicular networks, in which a rapid domain shift occurs frequently due to different channel impairments such as Doppler shift and multi-path fading. Mobility is a main culprit behind much of the dynamics in such networks. The presence of such mobility and dynamics creates challenges for multiple-input multiple-output (MIMO) signal detection. Conventional MIMO signal detection algorithms such as maximum likelihood detector (MLD), minimum mean square error (MMSE), zero-forcing (ZF) [1], and approximate message passing (AMP) [2] are model-driven, and require the knowledge of perfect channel state information (CSI). However, it is difficult to obtain accurate instantaneous CSI in a highly

dynamic environment due to high mobility. Consequently, the conventional algorithms designed in [1], [2] perform poorly under mobility, or they are too complex to be practical, as they treat the acquired imperfect CSI as if it were perfect.

Machine learning techniques [3]–[5] can be a promising approach to address these challenges, as shown in [6]–[9]. Indeed, several deep learning (DL) based approaches were proposed in [6]–[9] for MIMO signal detection, and they are shown to outperform conventional MIMO signal detection algorithms proposed in [1], [2]. However, the prior art in [6]–[9] relies on highly parameterized deep neural networks (DNN) models so as to represent a broad range of mappings for various channel realizations. As such, massive training samples in the order of hundreds of thousands to millions are typically required by the works in [6]–[9] in order to obtain a desirable mapping. Meanwhile, the dynamic nature of wireless channels, particularly in presence of mobility, causes a rapid domain shift for the communication signals. In such dynamic and mobile environment, DNNs trained for a given channel may no longer perform well on future unseen channel realizations. Thus, online training or fine-tuning is required by techniques like those in [6]–[9] in order to adapt to domain shifts. Dynamic settings, such as vehicular networks, cannot tolerate the waiting time associated with gathering a large number of training samples and online retraining, which incur significant end-to-end delay. In such settings if the information is time-critical (e.g., navigation in autonomous vehicles), the delay experienced by the system in order to adapt to new domains could lead to dire consequences. Clearly, there is a lack of existing approaches for MIMO signal detection that can overcome the grand challenge of enabling a wireless system to effectively adapt to dynamic environments, without the need for massive volumes of training samples and frequent online retraining.

The main contribution of this paper is a novel MIMO signal detection method that exploits a geodesic flow kernel (GFK) [10] for the purpose of learning domain shifts over Grassmannian manifolds. The GFK is particularly used in geometric support vector machine (G-SVM) for detecting MIMO signals in an unsupervised manner. Geometric approaches, including Grassmannian and Riemannian geometry, have been used to address challenges in wireless communication systems, such as the design of beamforming codebook in [11], wireless resource allocations [12]–[14] and deriving the capacity of the noncoherent multiple-antenna channel [15]. However, the

This research was supported by the Center for Assured and Resilient Navigation in Advanced Transportation Systems (CARNATIONS) under the US Department of Transportation (USDOT)'s University Transportation Center (UTC) program (Grant No. 69A3552348324).

works in [11]–[15] do not consider the Grassmannian geometry to study the MIMO signal detection under domain shift.

In our approach, we first represent the received MIMO signals as points on Grassmannian manifold by performing principal component analysis (PCA) [16] which identifies the subspaces where the variance of the received signals are maximized. Then, we show that the channel variations due to mobility flows along a geodesic between training and test data point which belong to different domains. The flow along the geodesic represents incremental changes in geometric and statistical properties of the received signals due to mobility. The geodesic flow kernel derives low-dimensional representations of the received MIMO signals over the Grassman manifold that are invariant to domain shift and used in G-SVM for MIMO signal detection. Simulation results shows that the proposed method achieves promising performance compared to the state-of-the-art baselines like OAMPNet [7], HyperMIMO [8] and MMNet [9] with only 1200 training samples and without online training.

The rest of this paper is organized as follows. The system model and problem formulation are presented in Section II. Section III presents the proposed learning-based MIMO signal detection method. Simulation results are presented in Section IV. Finally, conclusions are drawn in Section V.

II. SYSTEM MODEL AND PROBLEM FORMULATION

A. Preliminaries

A Grassmannian manifold $G_{T,N}$ is a set of N -dimensional subspaces in \mathbb{C}^T that can be used to define a smooth Riemannian manifold with geometric, differential and probabilistic structure, where T is the dimensionality of the original data [17]. A point P on $G_{T,N}$ is a subspace and is typically represented by a basis matrix spanning the subspace. The subspace can be computed by utilizing PCA [16]. PCA computes a subspace on the Grassmannian manifold by extracting the principal components (i.e., eigenvectors) from the covariance matrix of the input data. These principal components represent the most significant directions of variation in the data and form the basis for the subspace within the Grassmannian manifold.

B. System Model

We consider a high mobility uplink MIMO scenario consisting of M transmit antennas at mobile node (e.g., ground or aerial vehicle) and N receive antennas at the receiver (e.g., edge server). The mobile node transmits one out of Z possible encoded symbols $\mathbf{s}^{(i)} \in \mathbb{C}^{1 \times L}$ with $i \in \mathcal{Z} = \{1, 2, \dots, Z\}$. Each symbol $\mathbf{s}^{(i)}$ is a complex random variable with L being an integer multiple of M . Then, $\mathbf{s}^{(i)}$ can be divided into $1 \times T$ sub-vectors with $T = L/M$, i.e., $\mathbf{s}^{(i)} = [\mathbf{s}_1^{(i)}, \mathbf{s}_2^{(i)}, \dots, \mathbf{s}_M^{(i)}]$. Thus, the transmitted symbol $\mathbf{s}^{(i)}$ can be converted into a matrix $\mathbf{X}^{(i)} \in \mathbb{C}^{M \times T}$. In situations where L is not an integer multiple of M , zero-padding can be used to extend $\mathbf{s}^{(i)}$ to meet the integer-multiple constraint. Matrix $\mathbf{X}^{(i)} \in \mathbb{C}^{M \times T}$ is transmitted by the mobile node over T slots through M antennas.

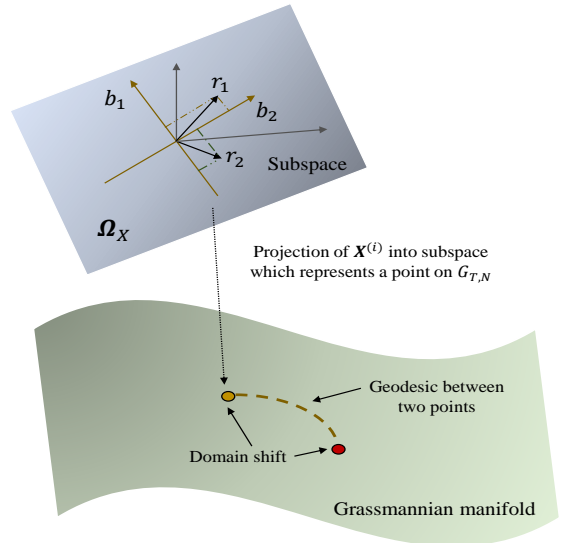


Fig. 1: An example of the transformation of coordinate system through the representation of data on Grassmannian manifolds. Here, $[b_1, b_2]$ is the basis of Ω_X , r_1, r_2 are the row vector of \mathbf{X} . $\mathbf{U}_X = [u_{i,j}]$ where $u_{i,j}$ is the length of the component of r_i in the direction of b_j .

High mobility leads to temporally-correlated MIMO channels. Under the assumption of rich scattering, classical Clark’s model [18] is used to quantify the level of channel temporal correlation associated with the node speed. We divide time into baseband sampling intervals, called time slots. Then, the realization of the slot- t MIMO channel from the mobile node to the receiver can be represented by $\mathbf{H}_t \in \mathbb{C}^{N \times M}$. To reflect that channel’s temporal variation, the transmitted symbol $\mathbf{X}^{(i)}$ can be written in terms of its columns, i.e., $\mathbf{X}^{(i)} = [\mathbf{x}_1^{(i)}, \mathbf{x}_2^{(i)}, \dots, \mathbf{x}_T^{(i)}]$. Then, the received signal at the receiver due to the transmission of $\mathbf{X}^{(i)}$ can be represented by matrix $\mathbf{Y}^{(i)} = [\mathbf{y}_1^{(i)}, \mathbf{y}_2^{(i)}, \dots, \mathbf{y}_T^{(i)}] \in \mathbb{C}^{N \times T}$ with

$$\mathbf{y}_t^{(i)} = \sqrt{P}\mathbf{H}_t^{(i)} \mathbf{x}_t^{(i)} + \mathbf{w}^{(i)}, \quad (1)$$

where P is the transmit power and $\mathbf{w}^{(i)}$ is the additive white Gaussian noise (AWGN) vector whose entries are assumed to be mutually independent with zero mean and variance γ_w , i.e., $w_i \sim \mathcal{N}(w_i, 0, \gamma_w^{-1})$. From (1), we observe that due to high mobility, the channel $\mathcal{H}^{(i)} = \{\mathbf{H}_t^{(i)}\}_{t=1}^T$ varies throughout the transmission duration of a single symbol across T time slots.

The transmitted signal $\mathbf{X}^{(i)} \in \mathbb{C}^{M \times T}$ can be represented as a point $\Omega_X^{(i)}$ on $G_{T,M}$ spanned by its row vector using PCA, along with a matrix $\mathbf{U}_X^{(i)} \in \mathbb{C}^{M \times M}$ which specifies the M row vectors of $\mathbf{X}^{(i)}$ with respect to a canonical basis in $\Omega_X^{(i)}$ [15]. The representation of the transmitted signal over Grassmannian manifolds $\mathbf{X}^{(i)} \rightarrow (\mathbf{U}_X^{(i)}, \Omega_X^{(i)})$ is the transformation of coordinate system $\mathbb{C}^{M \times T} \rightarrow \mathbb{C}^{M \times M} \times G_{T,M}$, as shown in Fig. 1. To understand the motivation of such representation, we first consider an extreme case without additive noise $\mathbf{W}^{(i)}$ such that $\mathbf{Y}^{(i)} = \mathcal{H}^{(i)} \mathbf{X}^{(i)}$. In this case, the row vectors of the received signals span the same subspace as $\mathbf{X}^{(i)}$, i.e., $\Omega_{\mathcal{H}\mathbf{X}}^{(i)} = \Omega_X^{(i)}$. This shows that the channel

$\mathcal{H}^{(i)}$ affects the transmitted signal $\mathbf{X}^{(i)}$ by changing $\mathbf{U}_{\mathbf{X}}^{(i)}$. In consequence, the position of the subspace of the transmitted signal shifts towards the direction of the change in $\mathbf{U}_{\mathbf{X}}^{(i)}$ over Grassmannian manifolds. For a channel with additive noise, $\mathbf{U}_{\mathbf{X}}^{(i)}$ is affected by both noise and channel and the $\Omega_{\mathbf{X}}^{(i)}$ is affected by noise only. In the high signal-to-noise-ratio (SNR) regime, the impact of noise is negligible compared to the variation in the channel. In this case, it can be intuitively assumed that $\mathbf{U}_{\mathbf{X}}^{(i)}$ is affected only by the channel [15].

C. Problem Formulation

Let \mathcal{Y} be input space of a dataset $\mathcal{D} = \{(Y_j | P_Y(Y_j))\}_{j=1}^K$, where $Y_j \in \mathcal{Y}$ is the input j and K is the total size of the dataset. When Y_j is seen as realization of random variables Y , then, it is possible to define a domain as its marginal distribution $P_Y(Y)$. If the domains of the training \mathcal{D}_r and test \mathcal{D}_s datasets are different, then $P_Y^s(Y) \neq P_Y^t(Y)$. In other words, the marginal distributions are different. From (1), this domain shift is associated with the distribution of the received signal which is caused by channel variation due to mobility.

To illustrate how representation over Grassmannian manifolds can assist in addressing the challenge of rapid domain shift under mobility, consider two subspaces are computed from the training and test dataset corresponding to its domain \mathcal{D}_r and \mathcal{D}_s , respectively. Those two subspaces are represented as two points on Grassmannian manifolds. For a static channel and zero noise, the two points are identical on $G_{T,M}$. In this case, the two domains are similar to each other, i.e., the training and test dataset are similarly distributed. In the presence of channel variation and noise, they are two different points on $G_{T,M}$ and hence, the two domains are far apart on the manifolds.

In real-world applications, it is very difficult to ensure that the training and test data are drawn from a similar domain. This problem is particularly challenging in dynamic wireless communication settings in which a rapid domain shift occurs frequently due to mobility. Hence, our overarching goal is to overcome the challenge of the domain shift problem by identifying meaningful intermediate subspaces computed from the training and the test dataset that are robust to channel variation due to mobility. Specifically, we intend to use these meaningful intermediate subspaces to predict the transmitted MIMO symbol that belongs to domain \mathcal{D}_s (i.e., under unseen channel realizations due to mobility) by only using the labeled training dataset that belongs to domain \mathcal{D}_r .

III. GFK BASED MODEL FOR MIMO SIGNAL DETECTION

As explained next, the proposed framework consists of the following steps: i) formulation of a geodesic flow curve connecting the training and test domains on the Grassmannian manifolds, ii) computing the GFK, and iii) use of the GFK in G-SVM classifier for MIMO signal detection.

A. Geodesic Flow for Domain Shift Adaptation

Since the symbol $\mathbf{s}^{(i)} \in \mathbb{C}^{1 \times L}$ is converted into matrix $\mathbf{X}^{(i)} \in \mathbb{C}^{M \times T}$ when transmitted over M antennas, it is first

converted back to its vector form, i.e., $\hat{\mathbf{s}}^{(i)} \in \mathbb{C}^{1 \times L'}$, where $L' = NT$ and $L' = L$ if $M = N$. This conversion is done by the concatenation of the row vectors of the received signal matrix $\mathbf{Y}^{(i)} \in \mathbb{C}^{N \times T}$. Then, PCA is applied to identify the subspace of the received symbol. Since the number of eigenvectors of the received signal is N , it is sufficient to represent a subspace through its orthonormal basis $\mathbf{S} \in \mathbb{C}^{L' \times N}$ by applying PCA, where L' is the dimension of the data (i.e., symbol), and N is the dimension of the subspace. To obtain meaningful intermediate subspaces between the training and test domains for handling a domain shift, a set of tools is required that is consistent with the geometry of the space spanned by these $L' \times N$ subspaces.

Let $\mathbf{S}_r, \mathbf{S}_s \in \mathbb{C}^{L' \times N}$ be two sets of orthonormal basis of the subspaces obtained by PCA from the received signals in the training and test domains. We define $\mathbf{R}_r \in \mathbb{C}^{L' \times (L' - N)}$ as the orthonormal complement to \mathbf{S}_r , namely $\mathbf{R}_r^\dagger \mathbf{S}_r = 0$, where \dagger is the Hermitian or matrix conjugate transpose. Using a canonical Euclidean metric for the Riemannian manifold in a Grassmannian manifold, the geodesic flow can be parametrized as $\Phi(q) : q \in [0, 1] \rightarrow \Phi(q) \in G_{L', N}$ with the constraint $\Phi(0) = \mathbf{S}_r$ and $\Phi(1) = \mathbf{S}_s$. Then, the geodesic flow that emanates from \mathbf{S}_r to \mathbf{S}_s will be given by [10]

$$\begin{aligned} \Phi(q) &= \mathbf{S}_r \mathbf{U}_1 \Gamma(q) - \mathbf{R}_r \mathbf{U}_2 \Sigma(q), \\ &= [\mathbf{S}_r \quad \mathbf{R}_r] \begin{bmatrix} \mathbf{U}_1 & 0 \\ 0 & \mathbf{U}_2 \end{bmatrix} \begin{bmatrix} \Gamma(q) \\ \Sigma(q) \end{bmatrix}, \end{aligned} \quad (2)$$

where $\mathbf{U}_1 \in \mathbb{C}^{N \times N}$ and $\mathbf{U}_2 \in \mathbb{C}^{(L' - N) \times N}$ are orthonormal matrices given by singular value decomposition (SVD) as follows:

$$\mathbf{S}_r^\dagger \mathbf{S}_s = \mathbf{U}_1 \Gamma \mathbf{V}^\dagger, \quad \mathbf{R}_r^\dagger \mathbf{S}_s = -\mathbf{U}_2 \Sigma \mathbf{V}^\dagger, \quad (3)$$

where $\Gamma \in \mathbb{C}^{N \times N}$ and $\Sigma \in \mathbb{C}^{N \times N}$ are diagonal matrices. The diagonal elements $\cos \phi_i$ and $\sin \phi_i$ for $i = 1, 2, \dots, N$ are called principle angles i.e., $0 \leq \phi_1 \dots \leq \phi_N \leq \pi/2$, and are the measure of degree of overlap between \mathbf{S}_r and \mathbf{S}_s . Based on (2), the geodesic flow can be viewed as a collection of infinite meaningful subspaces gradually varying from the training domain \mathcal{D}_r to the test domain \mathcal{D}_s with the variations being caused by the channel dynamics due to mobility. In other words, the channel variations flow along a geodesic between training and test data points which belong to different domains.

B. Computation of the Geodesic Flow Kernel

Let $\hat{\mathbf{s}}_r^{(i)}$ and $\hat{\mathbf{s}}_s^{(i)}$ be the two versions of the originally transmitted symbol $\mathbf{s}^{(i)}$ that are received, respectively, during the training and test phases. Those received symbols belong to different domains. We compute their projections on the geodesic $\Phi(q)$, i.e., $\Phi(q)^\dagger \hat{\mathbf{s}}^\dagger$, for a continuous q starting from 0 to 1, where 0 and 1 indicate the training domain and test domain, respectively. By using projection into all subspaces along the geodesic, we utilize a similarity measure that is robust to channel variations. In other words, the net effect of projections is a representation over Grassmannian manifolds that is invariant to the domain shift. All the projections are concatenated into infinite-dimensional feature vectors \mathbf{z}_r^∞ and

\mathbf{z}_s^∞ . Computationally, we do not need to compute infinitely many projections to define GFK. Instead, the GFK can be defined by inner products between \mathbf{z}_r^∞ and \mathbf{z}_s^∞ as:

$$\begin{aligned} \langle \mathbf{z}_r^\infty, \mathbf{z}_s^\infty \rangle &= \int_0^1 \left(\Phi(q)^\dagger (\hat{\mathbf{s}}_r^{(i)})^\dagger \right)^\dagger \left(\Phi(q)^\dagger (\hat{\mathbf{s}}_s^{(i)})^\dagger \right) dq \\ &= \hat{\mathbf{s}}_r^{(i)} \mathbf{F} (\hat{\mathbf{s}}_s^{(i)})^\dagger, \end{aligned} \quad (4)$$

where $\mathbf{F} \in \mathbb{C}^{L' \times L'}$ is a positive definite matrix

$$\mathbf{F} = \int_0^1 \Phi(q) \Phi(q)^\dagger dq. \quad (5)$$

The operation performed in (4) is the *kernel trick* [10], where a kernel function induces inner products between infinite-dimensional features without explicitly computing an infinite number of projections. Then, the geodesic flow kernel \mathbf{F} can be formulated in closed form as follows [10]:

$$\mathbf{F} = [\mathbf{S}_r \mathbf{U}_1 \quad \mathbf{R}_r \mathbf{U}_2] \begin{bmatrix} \Upsilon_1 & \Upsilon_2 \\ \Upsilon_2 & \Upsilon_3 \end{bmatrix} \begin{bmatrix} \mathbf{U}_1^\dagger \mathbf{S}_r^\dagger \\ \mathbf{U}_2^\dagger \mathbf{R}_r^\dagger \end{bmatrix}, \quad (6)$$

where Υ_1, Υ_2 , and Υ_3 are diagonal matrices, and the diagonal entries of these matrices are given by [10]

$$\sigma_{1j} = \int_0^1 \cos^2(q\phi_j) dq = 1 + \frac{\sin(2\phi_j)}{2\phi_j}, \quad (7)$$

$$\sigma_{2j} = \int_0^1 \cos(q\phi_j) \sin(q\phi_j) dq = \frac{\cos(2\phi_j) - 1}{2\phi_j}, \quad (8)$$

$$\sigma_{3j} = \int_0^1 \sin^2(q\phi_j) dq = 1 - \frac{\sin(2\phi_j)}{2\phi_j}, \quad (9)$$

respectively, and $j = 1, 2, \dots, N$.

C. GFK G-SVM for Signal Detection

Now, let $\{\mathcal{S}_r, \mathcal{T}_r\} = \{(\hat{\mathbf{s}}_r^l, \tau_r^l)\}_{l=1}^{n_r}$, with $\hat{\mathbf{s}}_r^l \in \mathbb{C}^{1 \times L'}$, and $\tau_r^l \in \mathcal{Z}$ be the set of n_r labeled training dataset corresponding to Z classes (i.e., Z possible symbols in alphabet \mathcal{Z}) from domain \mathcal{D}_r . We also define $\{\mathcal{S}_s\} = \{\hat{\mathbf{s}}_s^k\}_{k=1}^{n_s}$, $\hat{\mathbf{s}}_s^k \in \mathbb{C}^{1 \times L'}$ as the set of n_s unlabeled test dataset from domain \mathcal{D}_s . The classical approach to solving the multi-class SVM problem is to consider the problem as a collection of binary classification problems, where the z -th classifier constructs a hyperplane between class z and the rest of the $Z-1$ classes. Hence, using a Lagrangian formulation of the classical linearly constrained optimization problem, the final dual problem can be written as [19]:

$$\begin{aligned} \max_{\gamma} & \left\{ \sum_{l=1}^{n_r} \gamma_l - \frac{1}{2} \sum_{l=1}^{n_r} \sum_{l'=1}^{n_r} \gamma_l \gamma_{l'} \tau_r^l \tau_r^{l'} \mathbf{K} \left(\hat{\mathbf{s}}_r^l, \hat{\mathbf{s}}_r^{l'} \right) \right\}, \quad (10) \\ \text{s.t.} & \sum_{l=1}^{n_r} \tau_r^l \gamma_l, 0 \leq \gamma_l, \forall l = 1, 2, \dots, n_r, \end{aligned}$$

where the kernel matrix $\mathbf{K} \left(\hat{\mathbf{s}}_r^l, \hat{\mathbf{s}}_r^{l'} \right)$ is computed by (4). Then, the decision function for predicting the transmitted MIMO signal for any test symbol $\hat{\mathbf{s}}_s^k$ from $\{\mathcal{S}_s\}$ is given by [19],

$$\mathcal{F}(\hat{\mathbf{s}}_s^k) = \left(\sum_{l=1}^{n_{sv}} \gamma_l \tau_r^l \mathbf{K} \left(\hat{\mathbf{s}}_r^l, \hat{\mathbf{s}}_s^k \right) + b \right), \quad (11)$$

Algorithm 1 Overview of the proposed GFK G-SVM

- 1: **Inputs** : Training dataset $\{\mathcal{S}_r, \mathcal{T}_r\} = \{(\hat{\mathbf{s}}_r^l, \tau_r^l)\}_{l=1}^{n_r}$,
 - 2: $\hat{\mathbf{s}}_r^l \in \mathbb{C}^{1 \times L'}, \tau_r^l \in \{1, 2, \dots, Z\}$;
 - 3: Test data points $\{\mathcal{S}_s\} = \{\hat{\mathbf{s}}_s^k\}_{k=1}^{n_s}, \hat{\mathbf{s}}_s^k \in \mathbb{C}^{1 \times L'}$;
 - 4: **Training:**
 - 5: Represent the data on $\mathbb{G}_{L', N}$ through PCA: $\mathbf{S}_r, \mathbf{S}_s \in \mathbb{C}^{L' \times N}$;
 - 6: Compute the geodesic flow kernel \mathbf{F} as in (6);
 - 7: Compute the kernel matrix \mathbf{K} by (4) for \mathcal{S}_r from domain \mathcal{D}^{tr} ;
 - 8: Use the kernel matrix \mathbf{K} in G-SVM algorithm by solving (10);
 - 9:
 - 10: **Classification:**
 - 11: Return the predicted transmitted MIMO signal using (11);
-

where n_{sv} is the total number of support vectors, γ_l are the Lagrange multipliers and b is the bias.

The MIMO signal detection method based on the proposed GFK G-SVM is summarized in Algorithm 1. As shown in Algorithm 1, the geodesic flow kernel is only computed once during the training phase. During the test phase, the algorithm then simply uses the GFK in G-SVM for MIMO signal detection using (11). Hence, no online training is required during testing.

IV. SIMULATION RESULTS AND ANALYSIS

We consider $M = 2$ transmit antennas at the mobile node and $N = 4$ receive antenna at the receiver. The 4×2 channel is temporally correlated with the speed specified by the normalized Doppler shift $f_D T_s = 0.01$ for a node velocity of 66 miles per hour (mph), where T_s is the baseband sampling interval or time slot. In our simulation, we consider the symbol error rate (SER) as the learning performance. The symbol vectors are generated by the classic mixture of Gaussian (MoG) model [20] which is widely adopted in the machine learning literature. The number of classes is set as $Z = 12$ and the dimension of each data sample is set as $L = 48$. We generate 1,000 random samples for test dataset and all the results presented in this section are averaged over these 1,000 test samples.

A. Simulation Results

The average SER performance of various MIMO signal detection methods for a target SER performance, i.e., 10^{-3} , with 15 dB SNR is summarized in Table I. From Table I, we observe that the DNN based methods in [7]–[9] require large training samples in the order of hundreds of thousands to millions. Also, the methods in [7]–[9] require online training to achieve their target performance. In contrast, our proposed framework only requires 1,200 training samples and no online training is required. Moreover, the architectures of the DNN-based methods are comprised of large training parameters and many layers, while the proposed method does not have any free learning parameters to train and, hence, does not need online fine-tuning. The above observations suggest that the proposed GFK G-SVM is a promising solution for dynamic settings.

In Fig. 2, we compare the online training overhead of various MIMO signal detection methods for different node ve-

TABLE I: MIMO signal detection schemes for a target SER performance, i.e., 10^{-3} , for 15 dB SNR

Method	CSI Used	Number of Samples	Number of parameters	Number of layers	Online Training required	Approach
Proposed GFK G-SVM	No	1,200	/	/	No	GFK based
OAMPNet [7]	Yes	2,50,000	20	10	Yes	DNN
MMNet [9]	Yes	500,000	200	10	Yes	DNN
HyperMIMO [8]	Yes	25,00,000	1,600	8	Yes	DNN

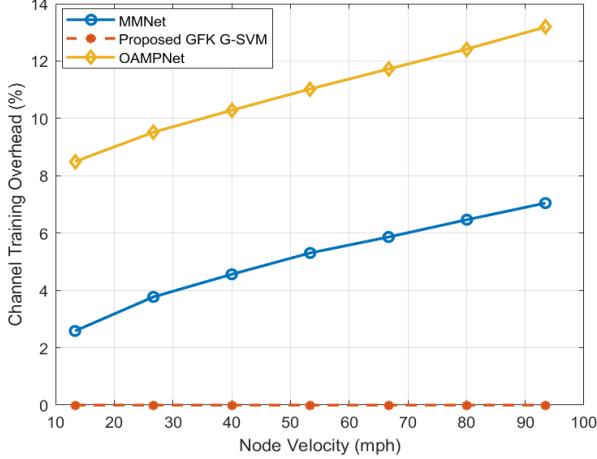


Fig. 2: The training overhead for obtaining CSI and online training versus node velocities for the target SER of 10^{-3} .

locities ranging from 13.33 mph to 93.42 mph, corresponding to the Doppler shifts ranging from 0.002 to 0.014 for a target SER performance of 10^{-3} . Under such dynamic settings, the DNN based methods in [7] and [9] need time to acquire CSI and use it for their online training for adapting to a domain shift. Let P be the time required for online training and F be the duration of the data frame. Then, the channel training overhead can be computed as $\frac{P}{P+F}$. From Fig. 2, we observe that the overhead of OAMPNet [7] and MMNet [9] increases monotonically with node velocity, as channel fading becomes faster which necessitates more frequent online training for these methods in [7] and [9]. In contrast, our proposed framework does not require channel training, thus avoiding this overhead. For instance, for a node velocity of 80.05 mph (i.e., Doppler shift of 0.012), the training overhead resulting from OAMPNet [7] and MMNet [9] is higher by about 12.41% and 6.46%, respectively, compared to our proposed framework that does not require channel training.

Next, in Fig. 3, we compare how our proposed framework performs under different Doppler shifts without any online training, compared to the DNN based methods in [7] and [9] which require online training. In particular, we compare the average SER performance for different normalized Doppler shifts ranging from 0.002 to 0.014, corresponding to node velocities ranging from 13.33 mph to 93.42 mph with a fixed SNR of 15 dB. From Fig. 3, we can see that the performance gap between the proposed method and the OAMPNet [7] increases in the range of moderate to large Doppler shift (i.e., above

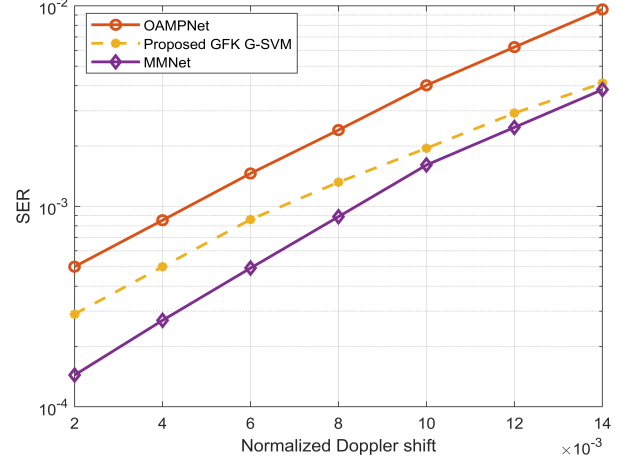


Fig. 3: Average SER performance for different Doppler shift with the average transmit SNR equal to 15 dB.

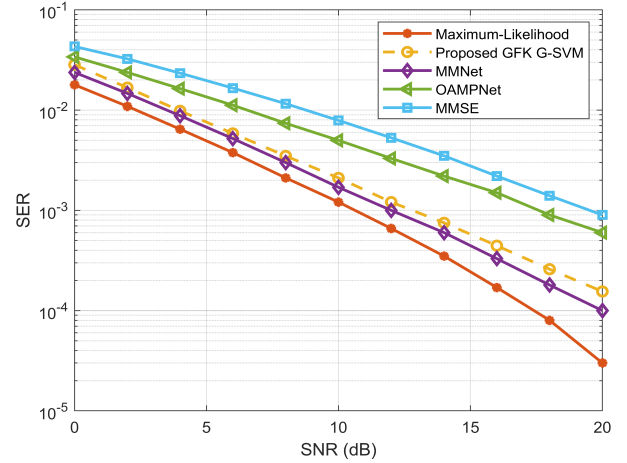


Fig. 4: Average SER performance for different average transmit SNR with the normalized Doppler shift fixed at 6×10^{-3} .

0.008). On the other hand, MMNet [9] achieves a slightly lower SER, compared to the proposed approach. However, as mentioned, MMNet [9] requires significant channel training overhead for online training, whereas our proposed framework does not need any online training, and hence, there is no channel training overhead.

Finally, in Fig. 4, we compare the average SER performance as a function of the SNR and with fixed normalized Doppler shift 0.006. From Fig. 4, we can see that the proposed method outperforms both the DNN based OAMPNet [7] and the traditional MMSE [1] approach with a large margin, reaching up to 82.75% and 74.13% better SER performance at 20 dB SNR than the MMSE [1] and OAMPNet [7], respectively. The performance is also comparable to MMNet [9] and the optimal maximum-likelihood detectors [1]. However, as mentioned, MMNet [9] requires a large volume of training samples as well as online training, whereas our proposed framework requires much fewer training samples and does not need online training. Moreover, the optimal maximum-likelihood detectors are highly computationally complex and require perfect CSI,

TABLE II: Computational complexity analysis.

Scheme	MMSE [1]	OAMPNet [7]	MMNet [9]	Maximum Likelihood [1]	Proposed GFK G-SVM
Data Features Extraction Complexity	/	Depends on layers and parameters	Depends on layers and parameters	/	Representation over manifold: $\mathcal{O}(N^2)$
Machine Learning Complexity	/	Scale as $\mathcal{O}(N^3)$	Scale as $\mathcal{O}(N^2)$	/	$\mathcal{O}(N) + \mathcal{O}(n_{SV}N)$
Total Complexity	$\mathcal{O}(N^3)$	$\mathcal{O}(N^3)$	$\mathcal{O}(N^2)$	$\mathcal{O}(N^3)$	$\mathcal{O}(N^2)$

which is extremely hard to get in such dynamic settings.

B. Computational Complexity Analysis

We next analyze the computational complexity of our proposed framework and compare it with other benchmark algorithms, as summarized in Table II. Our proposed approach is implemented in two steps: 1) computing the geodesic flow kernel over the Grassmannian manifolds, and 2) performing classification for MIMO signal detection. The computational complexity for computing the geodesic flow kernel over Grassmannian manifolds is $\mathcal{O}(N^2)$. Meanwhile, the computational complexity for G-SVM classification can be computed as

$$\mathcal{O}(n^2ZN) + \mathcal{O}(n_{SV}N) \approx \mathcal{O}(N), \quad (12)$$

where n is the number of training samples, Z is the number of classes, n_{SV} is the total number of support vectors, and N is the dimension of the subspace. Here, n , Z , and N are fixed for the proposed scheme. Thus, the total computational complexity of the proposed GFK G-SVM method scales as $\mathcal{O}(N^2)$, which is similar to the MMNet [9]. However, unlike MMNet [9], it does not require a large training sample and online training. Moreover, the computational complexity of our proposed framework is lower than MMSE [1], maximum-likelihood [1] and OAMPNet [7], as summarized in Table II.

V. CONCLUSION

In this paper, we have addressed the challenge of MIMO signal detection under rapid domain shifts in dynamic wireless communication settings. Towards this goal, we have proposed a novel GFK based MIMO signal detection method over Grassmannian manifolds. We have first represented the received MIMO signals as points on Grassmannian manifolds by formulating basis of subspaces spanned by the rows vectors of the received signal matrices. Then we have computed the GFK over the subspaces of the training and test data domains. As such, we have integrated an infinite number of subspaces that lie on the geodesic flow from the training subspace to the test one through GFK. We have shown that the flow along the geodesic represents incremental changes in geometric and statistical properties of the received signals due to mobility. By learning from all of these changes, the proposed GFK kernel can extract those representations that are invariant to the domain shift. Subsequently, we have used the kernel in G-SVM for MIMO signal detection. Simulation results show that the proposed method achieves competitive SER performance against the existing baselines like OAMPNet [7], HyperMIMO [8] and MMNet [9] with only 1,200 training samples and without online retraining.

REFERENCES

- [1] E.G. Larsson, "Mimo detection methods: How they work [lecture notes]," *IEEE Signal Processing Magazine*, vol. 26, no. 3, pp. 91–95, April, 2009.
- [2] C. Jeon, R. Ghods, A. Maleki, and C. Studer, "Optimality of large MIMO detection via approximate message passing," in *Proc. of the IEEE International Symposium on Information Theory (ISIT)*, Hong Kong, China, June, 2015, pp. 1227–1231.
- [3] M. Chen, U. Challita, W. Saad, C. Yin, and M. Debbah, "Artificial neural networks-based machine learning for wireless networks: A tutorial," *IEEE Communications Surveys & Tutorials*, vol. 21, no. 4, pp. 3039–3071, July, 2019.
- [4] C. Chaccour, W. Saad, M. Debbah, Z. Han, and H. V. Poor, "Less data, more knowledge: Building next generation semantic communication networks," *IEEE Communications Surveys & Tutorials*, to appear 2024.
- [5] W. Saad, O. Hashash, C. K. Thomas, C. Chaccour, M. Debbah, N. Mandayam, and Z. Han, "Artificial general intelligence (AGI)-native wireless systems: A journey beyond 6G," 2024.
- [6] N. Samuel, T. Diskin, and A. Wiesel, "Learning to detect," *IEEE Transactions on Signal Processing*, vol. 67, no. 10, pp. 2554–2564, February, 2019.
- [7] J. Liao, J. Zhao, F. Gao, and G. Y. Li, "A model-driven deep learning method for massive mimo detection," *IEEE Communications Letters*, vol. 24, no. 8, pp. 1724–1728, April, 2020.
- [8] M. Goutay, F. A. Aoudia, and J. Hoydis, "Deep hypernetwork-based mimo detection," in *Proc. of the IEEE 21st International Workshop on Signal Processing Advances in Wireless Communications (SPAWC)*, Atlanta, GA, USA, August, 2020, pp. 1–5.
- [9] M. Khani, M. Alizadeh, J. Hoydis, and P. Fleming, "Adaptive neural signal detection for massive MIMO," *IEEE Transactions on Wireless Communications*, vol. 19, no. 8, pp. 5635–5648, May, 2020.
- [10] B. Gong, Y. Shi, F. Sha, and K. Grauman, "Geodesic flow kernel for unsupervised domain adaptation," in *Proc. of the IEEE Conference on Computer Vision and Pattern Recognition*, Providence, RI, USA, June, 2012, pp. 2066–2073.
- [11] D.J. Love, R.W. Heath, and T. Strohmer, "Grassmannian beamforming for multiple-input multiple-output wireless systems," *IEEE Transactions on Information Theory*, vol. 49, no. 10, pp. 2735–2747, October, 2003.
- [12] R. Shelim and A. S. Ibrahim, "Learning wireless power allocation through graph convolutional regression networks over riemannian manifolds," *IEEE Transactions on Vehicular Technology*, vol. 73, no. 3, pp. 3652–3662, October, 2024.
- [13] R. Shelim and A. S. Ibrahim, "Wireless link scheduling over recurrent riemannian manifolds," *IEEE Transactions on Vehicular Technology*, vol. 72, no. 4, pp. 4959–4968, December, 2023.
- [14] R. Shelim and A. S. Ibrahim, "Geometric machine learning over riemannian manifolds for wireless link scheduling," *IEEE Access*, vol. 10, pp. 22854–22864, February, 2022.
- [15] L. Zheng and D. N. C. Tse, "Communication on the grassmann manifold: a geometric approach to the noncoherent multiple-antenna channel," *IEEE Transactions on Information Theory*, vol. 48, no. 2, pp. 359–383, February, 2002.
- [16] E.M. Mirkes, J. Bac, A. Fouché, S.V. Stassenko, A. Zinovyev, and A.N. Gorban, "Domain adaptation principal component analysis: base linear method for learning with out-of-distribution data," *Entropy*, vol. 25, no. 1, pp. 33, December, 2022.
- [17] P. Turaga, A. Veeraraghavan, A. Srivastava, and R. Chellappa, "Statistical computations on grassmann and stiefel manifolds for image and video-based recognition," *IEEE Transactions on Pattern Analysis and Machine Intelligence*, vol. 33, no. 11, pp. 2273–2286, April, 2011.

- [18] H. S. Rad and S. Gazor, "Space-time-frequency characterization of 3D nonisotropic MIMO multicarrier propagation channels employing directional antennas," *EURASIP Journal on Wireless Communications and Networking*, vol. 2008, pp. 1–14, August 2008.
- [19] F. F. Chamasemani and Y. P. Singh, "Multi-class support vector machine (svm) classifiers – an application in hypothyroid detection and classification," in *Proc. of the Sixth International Conference on Bio-Inspired Computing: Theories and Applications*, Penang, Malaysia, September, 2011, pp. 351–356.
- [20] G. J. McLachlan and S. Rathnayake, "On the number of components in a gaussian mixture model," *Wiley Interdisciplinary Reviews: Data Mining and Knowledge Discovery*, vol. 4, no. 5, pp. 341–355, September, 2014.